Applied Catalysis B: Environmental 140–141 (2013) 608–618

Contents lists available at SciVerse ScienceDirect

Applied Catalysis B: Environmental

journal homepage: www.elsevier.com/locate/apcatb

One-pot solvothermal syntheses of ternary heterostructured TiO_2–Bi_2MoO_6/$Bi_{3.64}Mo_{0.36}O_{6.55}$ controllable in terms of composition, morphology and structure: Materials of high visible-light driven photocatalytic activity

Jian-Ping Zou[a], Sheng-Lian Luo[a,*], Long-Zhu Zhang[a], Jun Ma[a], Si-Liang Lei[a], Long-Shuai Zhang[a], Xu-Biao Luo[a], Yan Luo[a], Gui-Sheng Zeng[a], Chak-Tong Au[a,b]

[a] Key Laboratory of Jiangxi Province for Persistent Pollutants Control and Resources Recycle, Nanchang Hangkong University, Nanchang, Jiangxi 330063, PR China

[b] Department of Chemistry, Hong Kong Baptist University, Kowloon Tong, Hong Kong, China

ARTICLE INFO

Article history:
Received 19 January 2013
Received in revised form 24 April 2013
Accepted 28 April 2013
Available online 8 May 2013

Keywords:
Bismuth molybdate
Composite materials
Controllable syntheses
Heterostructured
Photocatalysis

ABSTRACT

Novel ternary heterostructured TiO_2–Bi_2MoO_6/$Bi_{3.64}Mo_{0.36}O_{6.55}$ were synthesized by a one-pot template-free solvothermal method. For comparison studies, Bi_2MoO_6, $Bi_{3.64}Mo_{0.36}O_{6.55}$, Bi_2MoO_6/$Bi_{3.64}Mo_{0.36}O_{6.55}$, TiO_2–Bi_2MoO_6, and TiO_2–$Bi_{3.64}Mo_{0.36}O_{6.55}$ were also synthesized likewise. The photocatalysts were characterized by powder X-ray diffraction, UV–vis diffuse reflectance spectroscopy, scanning electron microscopy, transmission electron microscopy, and Raman spectroscopy. The experimental results showed that the composition, morphology and structure of the photocatalysts can be well controlled by adjusting the pH value, alcohol/water ratio, and TiO_2 content. Based on the findings, we put forward a mechanism for the formation of the materials. Furthermore, the results of photocatalytic degradation of Rhodamine B (RhB) and o-nitrophenol over the as-prepared materials indicate that photocatalytic efficiency can be closely related to the composition, morphology and structure of the materials. The ternary heterostructured 5%TiO_2–Bi_2MoO_6/$Bi_{3.64}Mo_{0.36}O_{6.55}$ exhibits good visible-light driven photocatalytic activity in the degradation of RhB and o-nitrophenol, much higher than those of TiO_2, Bi_2MoO_6, $Bi_{3.64}Mo_{0.36}O_{6.55}$, and any combination of the three. Finally, a new mechanism for the photocatalytic action of the heterostructured materials was put forward. Overall, the investigation provides a new reaction mode to explain the effective interfacial charge transfer and the significant improvement in photocatalytic efficiency of the ternary heterostructured composites.

1. Introduction

At the forefront of energy crisis and environmental pollution, semiconductor photocatalysis is expected to play a role in solving the urgent issues [1–6]. The photodecomposition of organic pollutants and the splitting of water using sunlight over semiconductor photocatalysts have attracted intense attention since the pioneering work of Honda and Fujishima on photoelectrochemical cell published in 1972 [7]. Subsequently, many types of photocatalysts have been reported, such as Fe_3O_4 [8], Cu_2O [9], $SrTiO_3$ [10], $BiSbO_4$ [11], Bi_2WO_6 [12], and BiOI [13]. Compared to single-component photocatalysts, the heterostructured semiconductor photocatalysts have received much more attention due to two reasons. First, the band gap of a heterostructured semiconductor can be well controlled through the change of catalyst composition. Second, charge transferring from one semiconductor to another can lead to efficient charge separation and subsequently reducing the chance of electron–hole pair recombination. It is because of these two factors the heterostructured semiconductor photocatalysts are superior to the single-component photocatalysts in photocatalytic performance. For example, Serpone et al. reported that the CdS/TiO_2 heterostructure exhibited good photocatalytic activity in the degradation of phenol and 2-chlorophenol [14]. Ke et al. showed that the WO_3/TiO_2 heterostructure displayed good photoactivity in the degradation of Rhodamine B (RhB) under UV light [15]. Besides, many other types of heterostructured semiconductors with good photocatalytic efficiency have been reported, such as TiO_2/BiOI [16], BiOCl/BiOI [17], Bi_2O_3/Bi_2WO_6 [18], BiOI/Bi_2O_3 [19], and Bi_2MoO_6/$Bi_{3.64}Mo_{0.36}O_{6.55}$ [20].

* Corresponding author. Tel.: +86 791 83863688; fax: +86 791 83953373.
E-mail address: sllou@hnu.edu.cn (S.-L. Luo).

0926-3373/$ – see front matter © 2013 Published by Elsevier B.V.
http://dx.doi.org/10.1016/j.apcatb.2013.04.057

In recent years, three-component systems have been found to exhibit high photocatalytic activity. For example, Tada et al. reported that CdS–Au–TiO_2 nanojunction system exhibited higher photocatalytic activity for degradation of methyl viologen than the single- and two-component systems [21]. It was reported that the high photocatalytic activity of Ag/AgBr/TiO_2 [22], Ag/AgBr/BiOBr [23], Ag/AgCl/ZnO [24] and AgBr–Ag–Bi_2WO_6 [25], that consist of two semiconductors and a transition metal was due to vectorial electron transfer driven by the two semiconductors in a process of two-step excitation. Besides, ZnO/$ZnWO_4$/WO_3 [26], WO_3/BiOCl/Bi_2O_3 [27], AgI/AgCl/TiO_2 [28], and CdS/ZnS/In_2S_3 [29], composed of three semiconductors, exhibit good photocatalytic activity for decomposition of organic pollutants or H_2 production in water splitting.

Bi_2MoO_6, as an important Aurivillius oxide, has attracted considerable attention because of its dielectric nature, catalytic behavior, and luminescence property [30–32]. Recent results revealed that Bi_2MoO_6 could function as an excellent photocatalyst for water splitting as well as for degradation of organic compounds under visible-light irradiation [33,34]. Till now, many studies have been carried out to clarify the effect of crystallinity, size, and morphology on photocatalytic performance of Bi_2MoO_6 that was hydrothermally synthesized [35]. To the best of our knowledge, however, investigations on heterostructured photocatalysts containing Bi_2MoO_6 are few, and there are no reports on three-component systems or ternary heterostructured composites that contain Bi_2MoO_6. In addition, despite it is known that beside pH value, factors such as alcohol/water ratio and TiO_2 content would have an effect on the crystallinity, size, and morphology of Bi_2MoO_6, and even on the composition and structure of the as-synthesized photocatalysts, research on this aspect has not been carried out.

In this study, ternary heterostructured photocatalyst TiO_2–Bi_2MoO_6/$Bi_{3.64}Mo_{0.36}O_{6.55}$ was synthesized by a facile one-pot solvothermal method. It was observed that factors such as pH value, ethanol amount, and TiO_2 loading content have influence on the composition, structure and morphology of TiO_2–Bi_2MoO_6/$Bi_{3.64}Mo_{0.36}O_{6.55}$. The effects of catalyst composition, structure and morphology on photocatalytic activity were also investigated. In addition, the photocatalytic degradation of RhB and o-nitrophenol under visible light irradiation using TiO_2–Bi_2MoO_6/$Bi_{3.64}Mo_{0.36}O_{6.55}$ were investigated in comparison with that using Bi_2MoO_6, $Bi_{3.64}Mo_{0.36}O_{6.55}$ as well as that using Bi_2MoO_6/$Bi_{3.64}Mo_{0.36}O_{6.55}$, TiO_2–Bi_2MoO_6 and TiO_2–$Bi_{3.64}Mo_{0.36}O_{6.55}$. The results reveal that the 5%TiO_2–Bi_2MoO_6/$Bi_{3.64}Mo_{0.36}O_{6.55}$ catalyst performs the best in the degradation of RhB and o-nitrophenol. Moreover, a new mechanism for the photocatalytic activity over ternary heterostructured TiO_2–Bi_2MoO_6/$Bi_{3.64}Mo_{0.36}O_{6.55}$ has been illustrated for the first time.

2. Experimental

2.1. Materials and measurement

All chemicals were analytically pure and used without further purification. The crystalline phases of samples were investigated by X-ray diffraction (Bruker D8 ADVANCE) using graphite monochromatized Cu $K\alpha$ (λ = 1.5406 Å) radiation. The XRD data for indexing and cell-parameter calculations were collected in a scan mode with a scanning speed of 2°/min in the 2θ range between 10° and 70°. The morphology of samples was studied with a scanning electron microscope (SEM, FEI, Holand) and a transmission electron microscope (TEM). Composition analyses on several randomly selected samples of the as-prepared catalysts were performed on a field-emission scanning electron microscope equipped with an energy dispersive X-ray spectroscope (EDS). The Ti/Bi molar ratio of as-prepared catalysts was estimated based on the averaged value of several randomly selected samples. The Ti/Bi molar ratio of the as-prepared samples were also determined based on ICP data collected over an inductively coupled plasma atomic emission spectrometer (ICP-AES; Vista-MPX, VARIAN) as well as those collected by means of X-ray fluorescence spectrometry (XRF) over a Panalytical Axios sequential spectrophotometer equipped with a rhodium radiation tube (samples in the form of pressed pellets). UV–vis diffuse reflectance spectra were measured with a PE Lambda 900 UV/vis spectrophotometer at room temperature. X-ray photoelectron spectroscopy (XPS) measurements were taken with a VG Escalab 250 spectrometer equipped with an Al anode (Al $K\alpha$ = 1486.7 eV). Raman measurements were performed using a JY LabRam HR800 spectrometer equipped with a microscope; laser radiation (λ = 514.5 nm; at 5 mW) was used as excitation source. Photoluminescence recording was performed on a Cary Edipse fluorescence spectrometer. The Brunauer–Emmett–Teller (BET) surface area of samples was measured by means of N_2 adsorption over a NOVA 2000e (Quantachrome) equipment.

Electrochemical measurements were performed on a CHI 660D electrochemical workstation (Shanghai Chenhua, China) using a standard three-electrode cell with a working electrode, a platinum wire as counter electrode, and a standard calomel electrode in saturated KCl as reference electrode. The working electrodes were prepared by dip-coating: 20 mg of photocatalyst was suspended in 5 mL ethanol (to produce a slurry), which was then dip-coated onto a 2 cm × 0.5 cm fluorine-tin oxide (FTO) glass electrode with a sheet resistance of 15 Ω. After drying under ambient condition, the films were sintered at 400 °C for 1 h. The electrolyte (0.1 M KOH or 0.5 M K_2SO_4) was purged with nitrogen. In photocurrent measurements, a 500 W xenon lamp with a 420 nm cutoff filter was used as the source of visible light irradiation and the other conditions were similar to those of electrochemical measurements.

2.2. Syntheses

2.2.1. Syntheses of Bi_2MoO_6, $Bi_{3.64}Mo_{0.36}O_{6.55}$ and Bi_2MoO_6/$Bi_{3.64}Mo_{0.36}O_{6.55}$

Bi_2MoO_6, $Bi_{3.64}Mo_{0.36}O_{6.55}$ and Bi_2MoO_6/$Bi_{3.64}Mo_{0.36}O_{6.55}$ of high purity were synthesized by solvothermal method. Through the addition of NaOH solution, the pH of the solution for the solvothermal reaction was adjusted for the generation of different materials: pH = 1.0–6.5 for Bi_2MoO_6; pH = 10.0–13.0 for $Bi_{3.64}Mo_{0.36}O_{6.55}$; and pH = 7.0–9.5 for Bi_2MoO_6/$Bi_{3.64}Mo_{0.36}O_{6.55}$. In a typical procedure, $Bi(NO_3)_3{\cdot}5H_2O$ (5 mmol) was dissolved in 10 mL distilled water under magnetic stirring for 30 min. Stoichiometric amounts of $(NH_4)_6Mo_7O_{24}{\cdot}4H_2O$ (0.36 mmol) was dissolved in 10 mL distilled water, and slowly added to the $Bi(NO_3)_3$ solution. Then 5 mL ethanol was added, and the pH of the mixed solution was adjusted through the adding of 10 mol/L NaOH solution to a designated value (pH = 1.0, 4.0, 6.0, 6.5, 7.0, 7.5, 8.0, 8.5, 9.0, 9.5, 10.0 and 13.0). After being stirred for 30 min at room temperature, the mixture was subject to ultrasonic treatment for 30 min and then to hydrothermal treatment in a 50 mL Teflon-lined stainless steel autoclave at 150 °C for 5 h. Finally, the obtained sample was calcined at 300 °C for 5 h.

2.2.2. Syntheses of heterostructured TiO_2–Bi_2MoO_6, TiO_2–$Bi_{3.64}Mo_{0.36}O_{6.55}$ and TiO_2–Bi_2MoO_6/$Bi_{3.64}Mo_{0.36}O_{6.55}$

Heterostructured TiO_2–Bi_2MoO_6, TiO_2–$Bi_{3.64}Mo_{0.36}O_{6.55}$ and TiO_2–Bi_2MoO_6/$Bi_{3.64}Mo_{0.36}O_{6.55}$ were prepared by the above method and procedures. The heterostructured TiO_2–Bi_2MoO_6/$Bi_{3.64}Mo_{0.36}O_{6.55}$ composites with different TiO_2 loadings were synthesized at pH = 7.5 or 9.5, and the TiO_2–Bi_2MoO_6 and TiO_2–$Bi_{3.64}Mo_{0.36}O_{6.55}$ composites are both with 5% TiO_2 loading (based on Ti/Bi molar ratio). Typically, $Bi(NO_3)_3{\cdot}5H_2O$ (5 mmol)

was dissolved in 10 mL distilled water under magnetic stirring for 30 min. Then a stoichiometric amount of $(NH_4)_6Mo_7O_{24}{\cdot}4H_2O$ (0.36 mmol) was dissolved in 10 mL distilled water, and the $(NH_4)_6Mo_7O_{24}$ solution was slowly added to the $Bi(NO_3)_3$ solution. In order to achieve a designated Ti/Bi ratio, tetrabutyl titanate dissolved in 5 mL ethanol was added. For example, the Ti/Bi molar ratio of 5%TiO_2–Bi_2MoO_6/$Bi_{3.64}Mo_{0.36}O_{6.55}$ was adjusted to 5% by this approach. Then procedure similar to that for the generation of Bi_2MoO_6 was followed to afford the formation of the heterostructured photocatalyst. Finally, the obtained samples were calcined at 300 °C for 5 h. Hereinafter, the heterostructured Bi_2MoO_6/$Bi_{3.64}Mo_{0.36}O_{6.55}$ loaded with 2.5%, 5.0%, 7.5%, and 10.0% TiO_2 synthesized at pH = 7.5 are denoted as 2.5TBM, 5TBM, 7.5TBM and 10TBM, respectively.

2.2.3. Syntheses of heterostructured Bi_2MoO_6/$Bi_{3.64}Mo_{0.36}O_{6.55}$ composites in solution different in ethanol/water ratio

The Bi_2MoO_6/$Bi_{3.64}Mo_{0.36}O_{6.55}$ composites with different compositions were prepared solvothermally at pH = 9.0 through the adjustment of $V_{ethanol}/V_{water}$ ratio in the mixed solution. In a typical procedure for the preparation of Bi_2MoO_6/$Bi_{3.64}Mo_{0.36}O_{6.55}$, the $V_{ethanol}/V_{water}$ ratio was adjusted to 3/2. First, $Bi(NO_3)_3{\cdot}5H_2O$ (5 mmol) was dissolved in 10 mL distilled water under magnetic stirring for 30 min and a stoichiometric amount of $(NH_4)_6Mo_7O_{24}{\cdot}4H_2O$ (0.36 mmol) was dissolved in 10 mL ethanol, and the latter was slowly added to the former, followed by the addition of 5 mL ethanol, and pH of the solution was adjusted to 9.0 with 10 mol/L NaOH solution. Then procedure similar to that of Bi_2MoO_6 synthesis was followed to afford the heterostructured photocatalyst. Other Bi_2MoO_6/$Bi_{3.64}Mo_{0.36}O_{6.55}$ that were different in composition were synthesized following the same procedure with the $V_{ethanol}/V_{water}$ ratio adjusted to 1/4, 2/3 and 4/1, respectively.

2.3. Photocatalytic reactions

Photocatalytic activities of the materials were evaluated in the degradation of RhB and o-nitrophenol under visible-light irradiation. A 100 W Xe lamp was used as visible-light source, and a 420 nm cutoff filter was placed above the reactor to cut off UV light. In the experiment, 0.1 g photocatalyst was added to 100 mL 1×10^{-5} mol/L RhB solution or 100 mL 5×10^{-5} mol/L o-nitrophenol. Prior to irradiation, the suspension was kept in the dark under stirring for 1 h to ensure adsorption/desorption equilibrium. During the experiment, 2 mL aliquots were collected at intervals from the suspension for the determination of RhB or o-nitrophenol concentration by UV–vis spectrophotometer (Cary 300 spectrophotometer) after immediate centrifugation.

3. Results and discussion

3.1. Materials characterization

Fig. 1 shows the XRD patterns of bismuth molybdate samples prepared at different pH values. All relevant peaks are identified and indexed based on the available JCPDS (Joint Committee for Powder Diffraction Studies) data. The materials obtained at pH of 1.0 and 6.5 are similar in crystal structure and can be identified as layered perovskite Bi_2MoO_6 (JCPDS No. 00-021-0102), while the materials obtained at pH of 10.0 and 13.0 exhibit crystal structure of perovskite $Bi_{3.64}Mo_{0.36}O_{6.55}$ (JCPDS No. 00-043-0446). When the pH value is varied from 7.0 to 9.5, there are the mixed phases of Bi_2MoO_6 and $Bi_{3.64}Mo_{0.36}O_{6.55}$. In all the three cases, there is no detection of any peaks attributable to impurities. It is worth pointing out that with increase of pH value from 7.5 to 9.5, the peaks of $Bi_{3.64}Mo_{0.36}O_{6.55}$ become broader while the peaks of Bi_2MoO_6 become narrower (Fig. 1), indicating that Bi_2MoO_6 formation is favored under acidic condition while $Bi_{3.64}Mo_{0.36}O_{6.55}$ formation is favored under base condition. Such a phenomenon was observed by Ren et al. [20] in the synthesis of $Bi_{3.64}Mo_{0.36}O_{6.55}$ within a narrow pH range of 6.6 to 7.0, but the formation mechanism of the mixed phases (i.e. Bi_2MoO_6 and $Bi_{3.64}Mo_{0.36}O_{6.55}$) was not given.

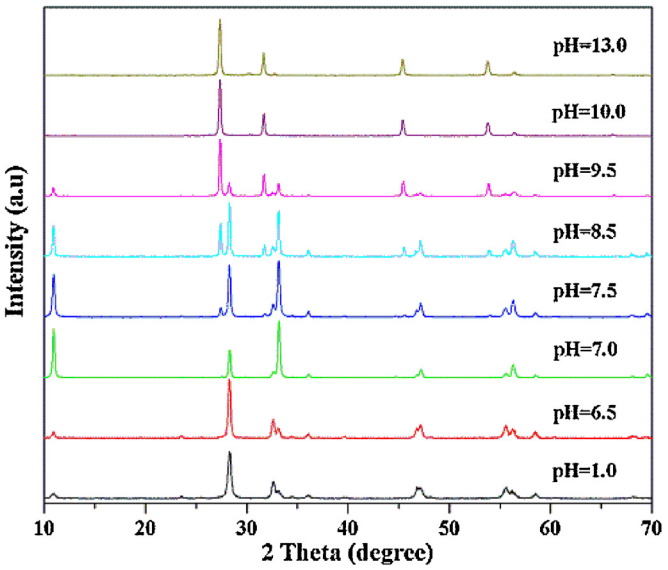

Fig. 1. XRD patterns of bismuth molybdate prepared at different pH values.

Fig. 2 shows the XRD patterns of Bi_2MoO_6/$Bi_{3.64}Mo_{0.36}O_{6.55}$ loaded (at pH = 7.5) with different amounts of TiO_2. There are the phases of Bi_2MoO_6 and $Bi_{3.64}Mo_{0.36}O_{6.55}$ in the heterostructured TiO_2–Bi_2MoO_6/$Bi_{3.64}Mo_{0.36}O_{6.55}$ composites, and there is no sight of any TiO_2 phase even up to a TiO_2 loading of 10%. When Bi_2MoO_6 and $Bi_{3.64}Mo_{0.36}O_{6.55}$ (synthesized at pH = 6.5 and 10.0, respectively) are loaded with TiO_2, there is no detection of the TiO_2 phase as well (Figs. S1 and S2 in Supporting information). Nonetheless, the presence of TiO_2 in the heterostructured composites is evidenced by means of XRF and the values are summarized

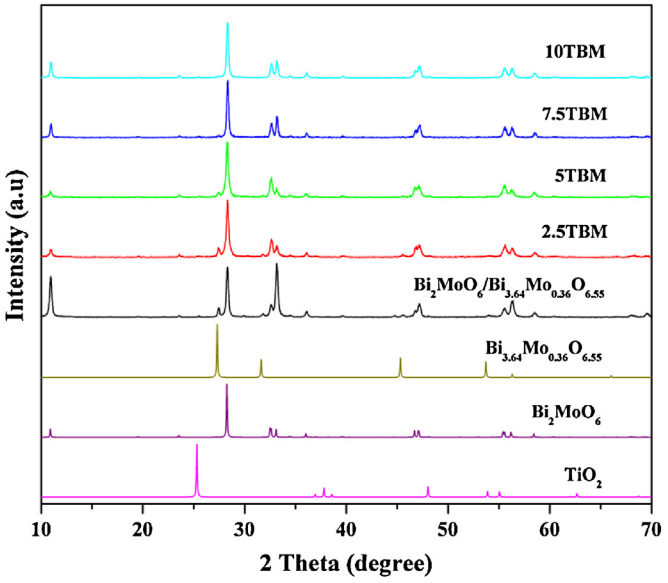

Fig. 2. XRD patterns of Bi_2MoO_6/$Bi_{3.64}Mo_{0.36}O_{6.55}$ loaded with different amounts of TiO_2 at pH = 7.5. Also shown are the XRD patterns of TiO_2, Bi_2MoO_6, $Bi_{3.64}Mo_{0.36}O_{6.55}$, and Bi_2MoO_6/$Bi_{3.64}Mo_{0.36}O_{6.55}$.

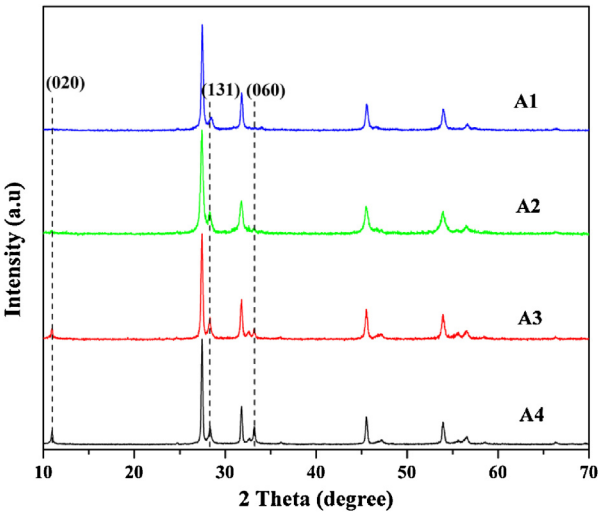

Fig. 3. XRD patterns of bismuth molybdate prepared at pH = 9 in solutions of different ethanol-to-water (volume) ratios: A1: $V_{ethanol}/V_{water}$ = 1/4 ($V_{ethanol}$ = 5 mL); A2: $V_{ethanol}/V_{water}$ = 2/3, ($V_{ethanol}$ = 10 mL); A3: $V_{ethanol}/V_{water}$ = 3/2 ($V_{ethanol}$ = 15 mL); A4: $V_{ethanol}/V_{water}$ = 4 ($V_{ethanol}$ = 20 mL).

in Table S1 (Supporting information). The molar contents of TiO_2 measured by XRF and EDS reasonably fit with the nominal values described in the experimental section. In addition, with increase of TiO_2 loading, the XRD peaks of $Bi_{3.64}Mo_{0.36}O_{6.55}$ phase in the heterostructured TiO_2–Bi_2MoO_6/$Bi_{3.64}Mo_{0.36}O_{6.55}$ composite become narrower, and the peaks of the $Bi_{3.64}Mo_{0.36}O_{6.55}$ phase disappear completely when TiO_2 loading reaches 10%. In other words, at 10% TiO_2 loading, 10%TiO_2–Bi_2MoO_6/$Bi_{3.64}Mo_{0.36}O_{6.55}$ (10TBM) is in fact a binary heterostructured 10%TiO_2–Bi_2MoO_6 composite. The result shows that phase transition of $Bi_{3.64}Mo_{0.36}O_{6.55}$ to Bi_2MoO_6 occurs as a result of TiO_2 loading. It is hence possible to fabricate TiO_2–Bi_2MoO_6/$Bi_{3.64}Mo_{0.36}O_{6.55}$ composites that are different in phase component as well as in property by regulating the loading of TiO_2. For the first time, an effective and facile way besides pH control is discovered for the control of phase composition in the preparation of this class of novel heterostructured compounds.

The effects of ethanol-to-water volume ratio of solvent on phase formation of the Bi_2MoO_6/$Bi_{3.64}Mo_{0.36}O_{6.55}$ composites were also studied. Fig. 3 shows the XRD patterns of the bismuth molybdate samples prepared at pH = 9 in solvent of different compositions of ethanol and water. It is obvious that the XRD patterns change with ethanol/water ratio. The characteristic (0 2 0), (1 3 1) and (0 6 0) peaks of Bi_2MoO_6 phase appear and increase in intensity with increasing content of ethanol. The result indicates that ethanol promotes the formation of Bi_2MoO_6 phase, and the Bi_2MoO_6-to-$Bi_{3.64}Mo_{0.36}O_{6.55}$ composition can be tuned by controlling the ethanol-to-water ratio. This is another way to achieve controllable syntheses of Bi_2MoO_6/$Bi_{3.64}Mo_{0.36}O_{6.55}$ or heterostructured TiO_2–Bi_2MoO_6/$Bi_{3.64}Mo_{0.36}O_{6.55}$ in terms of component, morphology and photocatalytic activity. The mechanistic roles of pH value, TiO_2 loading, and ethanol contents in the formation of bismuth molybdate will be discussed later in the section of formation mechanism.

Fig. S3 shows the Raman spectra of the heterostructured Bi_2MoO_6/$Bi_{3.64}Mo_{0.36}O_{6.55}$ composites 2.5TBM and 5TBM synthesized at pH = 7.5. The Raman spectra of 2.5TBM and 5TBM are nearly identical and show a very strong band at 795 cm^{-1} assignable to the A_{1g} mode of MoO_6 octahedron ascribable to O—Mo—O symmetric stretching [36,37]. The peaks in the range of 600–1000 cm^{-1} can be assigned to the stretching modes of Mo—O bands. There is no detection of bands that are attributable to TiO_2 in the Raman spectra of 2.5TBM and 5TBM [30]. The result can be explained based on the fact that the characteristic band of TiO_2 (at 150 cm^{-1}) relating to the O—Ti—O symmetric stretching overlaps with the bands of Bi_2MoO_6/$Bi_{3.64}Mo_{0.36}O_{6.55}$ (Fig. S3).

The typical full scan and high-resolution Ti-2p, O-1s, Mo3d, and Bi-4f spectra of 5TBM are shown in Fig. S4(a)–S4(e). One can see that the surface of 5TBM is only composed of Ti, O, Mo and Bi elements. Again the carbon can be ascribed to adventitious hydrocarbon. High-resolution XPS spectrum of Ti-2p region is shown in Fig. S4(b). The peaks centered at 463.9 and 457.8 eV are assigned to Ti-$2p_{1/2}$ and Ti-$2p_{3/2}$, respectively, in consistent with those of TiO_2 reported in the literature [38]. The O-1s band can be deconvoluted into two components as shown in Fig. S4(c). The peak at 529.7 eV can be assigned to Ti—O in TiO_2 [39], whereas the peaks located at 532.7 eV can be ascribed to the oxygen attached to bismuth and molybdenum (Bi—O and Mo—O bonds) in Bi_2MoO_6 or $Bi_{3.64}Mo_{0.36}O_{6.55}$ [40,41]. The results demonstrate that there are TiO_2 species in 5TBM, in consistent with the Raman results. As shown in Fig. S4(d), the peaks with binding energies around 235.1 and 231.9 eV can be ascribed to Mo-3d, indicating that the Mo species of 5TBM is hexavalent [42]. Similarly, the peaks centered at 163.9 and 158.6 eV (Fig. S4(e)) can be assigned to Bi-4f, indicating that the Bi species of 5TBM is trivalent. On the other hand, according to the XPS results, the concentration of surface Bi^{3+} is 15.7% (atom%), whereas that of Mo^{6+} is 6.46% (atom%). The atomic ratio of Bi and Mo is about 2.43, larger than the stoichiometric ratio of Bi_2MoO_6. The result reveals the existence of $Bi_{3.64}Mo_{0.36}O_{6.55}$ species, in agreement with the deduction based on XRD results.

The morphology of bismuth molybdate samples with 5% TiO_2 prepared at different pH values (pH = 6.5, 7.5, 9.0, and 10.0, respectively) were investigated by SEM and TEM. As shown in Fig. 4, the samples are different in morphology. With rise of pH values, there is rise in the number of nanoparticles but decrease in the number of flower-like nanosheets. At a pH value of 6.5, one can see flower-like superstructures with diameters of 0.5–1.0 μm (Fig. 4a). At pH = 7.5, besides the flower-like nanosheets, there is the presence of a small amount of nanoparticles (Fig. 4b). At pH = 9.0, nanoparticles are in majority and there is still a small amount of flower-like superstructures (Fig. 4c). At pH = 10.0, there is no detection of flower-like nanosheets and the material exists in the form of nanoparticles (Fig. 4d). The influence of pH value on morphology can be explained based on the results of XRD analysis. As shown in Fig. 1, at low pH values (pH < 8.5), Bi_2MoO_6 exists as major component in the Bi_2MoO_6/$Bi_{3.64}Mo_{0.36}O_{6.55}$ composite; with rise of pH value (8.5 < pH < 10), there is rise in the amount of $Bi_{3.64}Mo_{0.36}O_{6.55}$ in the composite. Because Bi_2MoO_6 and $Bi_{3.64}Mo_{0.36}O_{6.55}$ are different in shape, Bi_2MoO_6/$Bi_{3.64}Mo_{0.36}O_{6.55}$ morphology changes gradually from flower-like nanosheets (Bi_2MoO_6) to nanoparticles ($Bi_{3.64}Mo_{0.36}O_{6.55}$) (Fig. 4).

Fig. 5 shows the SEM images of bismuth molybdate without TiO_2 loading prepared at pH = 9 in mixed solutions of different ethanol-to-water ratios. At $V_{ethanol}/V_{water}$ = 1/4, there is a lot of $Bi_{3.64}Mo_{0.36}O_{6.55}$ nanoparticles and the co-existence of a small amount of Bi_2MoO_6 nanosheets (Fig. 5a). With rise of $V_{ethanol}/V_{water}$ ratio, more nanosheets can be seen (Fig. 5b and c). At $V_{ethanol}/V_{water}$ = 4, only Bi_2MoO_6 nanosheets exist (Fig. 5d).

The effect of TiO_2 loading on the morphology of bismuth molybdate was also studied. Fig. 6 are the SEM images of bismuth molybdate (at pH = 7.5) loaded with different amounts of TiO_2. With increase of TiO_2 loading, there is decline in the number of $Bi_{3.64}Mo_{0.36}O_{6.55}$ nanoparticles, and the formation and concurrent number rise of Bi_2MoO_6 flower-like nanosheets. In Fig. 6b, one can see the co-existence of nanoparticles and flower-like nanosheets in the 5TBM sample (TiO_2 loading = 5%). The co-presence of nanosheets and nanoparticles in 5TBM is also observed in the TEM images (Fig. 7a). In other words, there is the co-presence

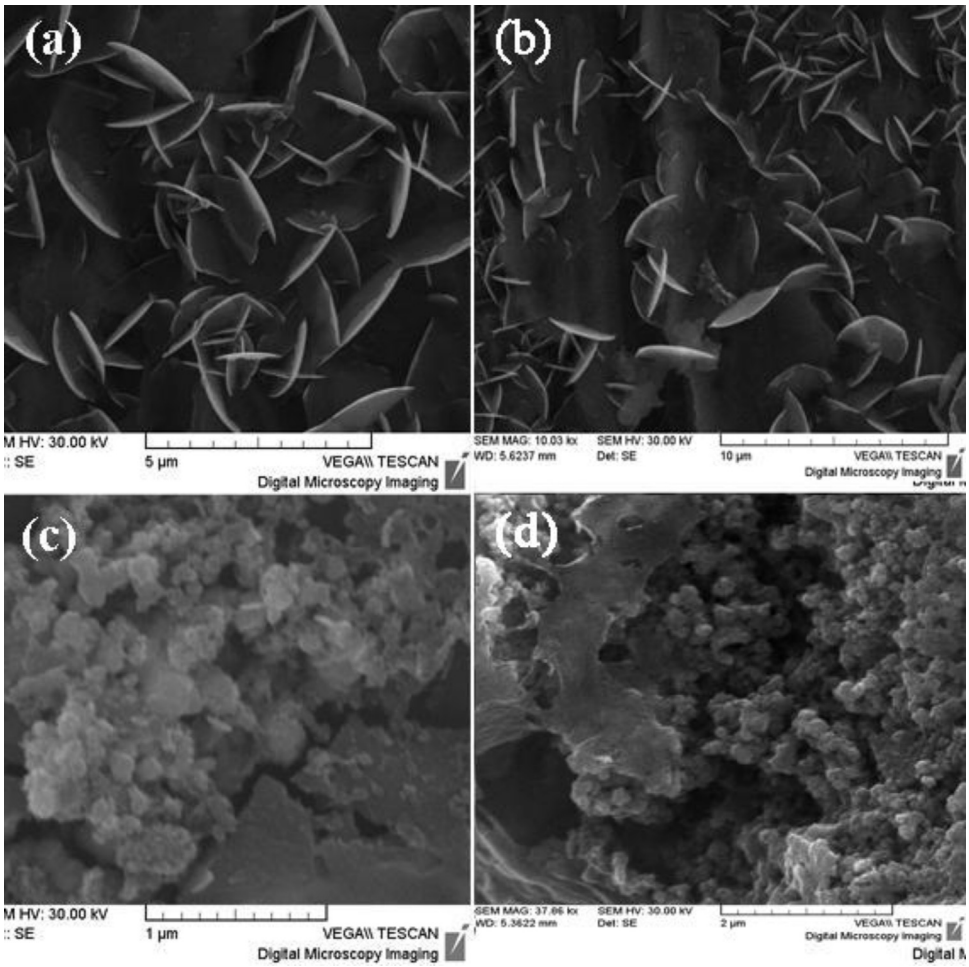

Fig. 4. SEM images of bismuth molybdate loaded with 5% TiO_2 at pH values of (a) 6.5, (b) 7.5, (c) 9.0 and (d) 10.0.

of $Bi_{3.64}Mo_{0.36}O_{6.55}$ and Bi_2MoO_6 in 5TBM. It is observed in Fig. 6d that when the amount of TiO_2 is 10%, there is the complete disappearance of nanoparticles and the sole presence of flower-like nanosheets (Fig. 6d). The HRTEM image (Fig. 7b) of 5TBM also shows the co-presence of Bi_2MoO_6, $Bi_{3.64}Mo_{0.36}O_{6.55}$ and TiO_2. The fringes of 0.278 and 0.312 nm are corresponding to the (1 3 1) plane of Bi_2MoO_6 and (1 1 1) plane of $Bi_{3.64}Mo_{0.36}O_{6.55}$, respectively, whereas that of 0.249 nm is corresponding to the (1 0 1) plane of TiO_2. The result demonstrates that there are separate TiO_2 nanoparticles on the surface of Bi_2MoO_6 nanosheets as well as the existence of heterojunctions between Bi_2MoO_6, $Bi_{3.64}Mo_{0.36}O_{6.55}$ and TiO_2, in consistent with the deduction based on the results of XPS and Raman analyses.

The effects of ethanol and TiO_2 loading on the morphology of bismuth molybdate (prepared at pH = 7.5) can also be explained based on the change of phase of bismuth molybdate components. Based on the results of XRD analyses, we know that with increase of ethanol/water ratio and TiO_2 loading, there is decline of $Bi_{3.64}Mo_{0.36}O_{6.55}$ phase in heterostructured TiO_2–Bi_2MoO_6/$Bi_{3.64}Mo_{0.36}O_{6.55}$. When ethanol/water ratio and TiO_2 content reach 4 and 10%, respectively, there is the complete disappearance of the $Bi_{3.64}Mo_{0.36}O_{6.55}$ phase. Therefore, similar to the effect of pH value on morphology, with rise of ethanol/water ratio and TiO_2 loading from 1/4 to 4 and 2.5% to 10%, respectively, sample morphology gradually changes from nanoparticles of $Bi_{3.64}Mo_{0.36}O_{6.55}$ to flower-like nanosheets of Bi_2MoO_6. To the best of knowledge, such effects of ethanol/water ratio and TiO_2 loading on the composition, structure and morphology of bismuth molybdate have never been reported before.

To study the optical absorption properties of the photocatalysts, UV–vis reflectance spectra of the as-prepared materials were recorded and are shown in Fig. S5. All the samples exhibit strong absorption in the visible region and the absorption edges are approximately at 500 nm. As shown in Fig. S6, according to the Kubelka–Munk method [43], the band gaps are ca. 2.55, 2.60, 2.58, 2.62, 2.68 and 2.70 eV for Bi_2MoO_6 (pH = 6.5), 5%TiO_2–Bi_2MoO_6 (pH = 6.5), Bi_2MoO_6/$Bi_{3.64}Mo_{0.36}O_{6.55}$ (pH = 7.5), 5TBM (pH = 7.5), $Bi_{3.64}Mo_{0.36}O_{6.55}$ (pH = 10.0) and 5%TiO_2–$Bi_{3.64}Mo_{0.36}O_{6.55}$ (pH = 10.0), respectively. It was observed that Bi_2MoO_6, $Bi_{3.64}Mo_{0.36}O_{6.55}$ and Bi_2MoO_6/$Bi_{3.64}Mo_{0.36}O_{6.55}$ as well as those of them loaded with TiO_2 have similar band gap values.

3.2. Formation mechanism

According to the results of XRD analysis, it is apparent that one can control the structure and morphology of bismuth molybdate by regulating the pH value. Generally, bismuth molybdate exists in two different phases, Bi_2MoO_6 with layered perovskite structure and $Bi_{3.64}Mo_{0.36}O_{6.55}$ with perovskite structure. Under the acidic condition, the formation of Bi_2MoO_6 is favorable, and the suggested chemical processes are:

$$Bi(NO_3)_3 + H_2O \overset{\text{hydrolysis}}{\longleftrightarrow} BiO(NO_3) + 2H^+ + 2NO_3^- \quad (1)$$

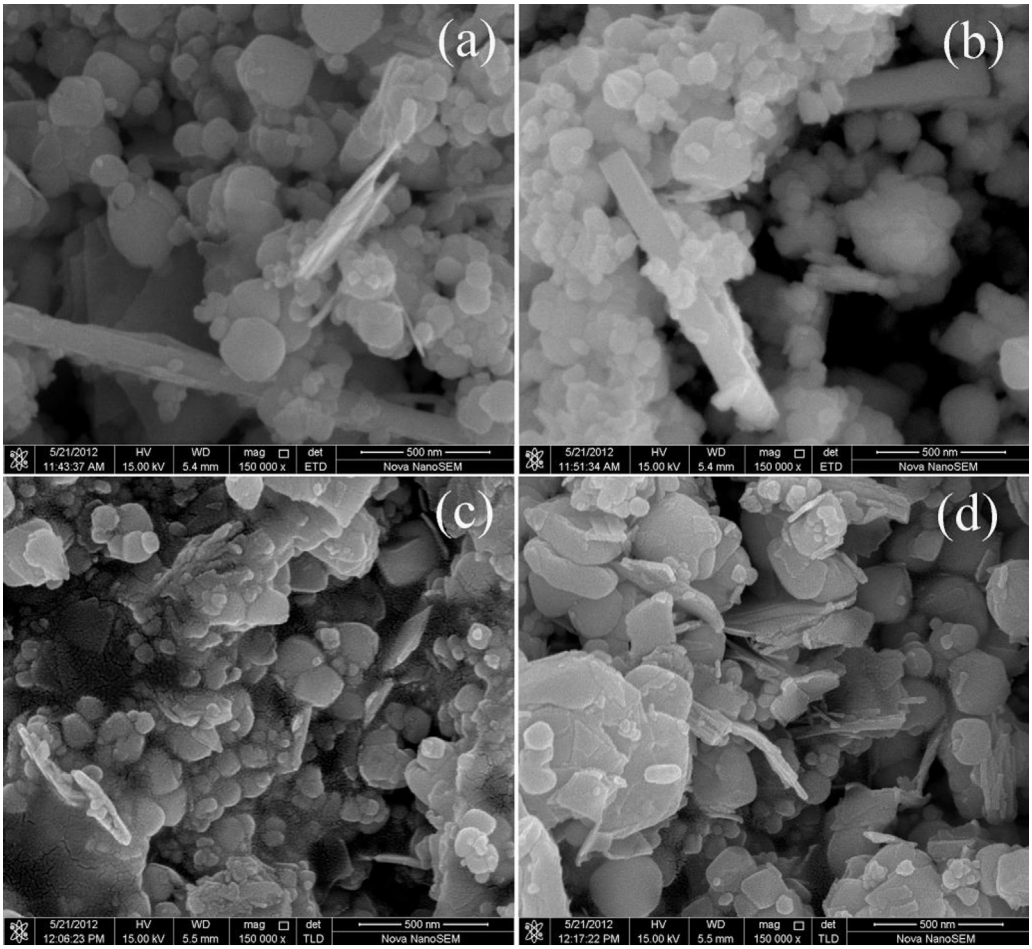

Fig. 5. SEM images of bismuth molybdate prepared at pH = 9 in solutions of different ethanol-to-water (volume) ratios: (a) $V_{ethanol}/V_{water}$ = 1/4 ($V_{ethanol}$ = 5 mL); (b) $V_{ethanol}/V_{water}$ = 2/3, ($V_{ethanol}$ = 10 mL); (c) $V_{ethanol}/V_{water}$ = 3/2 ($V_{ethanol}$ = 15 mL); (d) $V_{ethanol}/V_{water}$ = 4 ($V_{ethanol}$ = 20 mL).

$$2BiO(NO_3) + H_2O \overset{hydrolysis}{\longleftrightarrow} Bi_2O_2(OH)(NO_3) + H^+ + NO_3^- \quad (2)$$

$$(NH_4)_6Mo_7O_{24}\cdot 4H_2O + 6H^+ = 7H_2MoO_4 \cdot 6NH_4^+ \quad (3)$$

With the addition of ammonium molybdate, there is the formation and loading of H_2MoO_4 on the $Bi_2O_2(OH)(NO_3)$ compound [44,45]. Finally, the Bi_2MoO_6 product is synthesized through the solvothermal reaction:

$$Bi_2O_2(OH)(NO_3) + H_2MoO_4 \overset{solvothermal}{\longrightarrow} Bi_2MoO_6 + H^+ + NO_3^- + H_2O \quad (4)$$

Under base condition (pH > 7.0), MoO_4^- can independently exist in the solution, and the formation of $Bi_{3.64}Mo_{0.36}O_{6.55}$ becomes favorable. The related chemical processes are suggested as follows:

$$Bi_2O_2(OH)(NO_3) + MoO_4^{2-} \xrightarrow{solvothermal} Bi_{3.64}Mo_{0.36}O_{6.55} + OH^- + NO_3^- \quad (5)$$

$$Bi_2O_2(OH)(NO_3) + MoO_4^{2-} \overset{solvothermal}{\longrightarrow} Bi_{3.64}Mo_{0.36}O_{6.55} + OH^- + NO_3^- \quad (6)$$

The presence of ethanol in the mixed solution is found propitious for the formation of Bi_2MoO_6. Similar to the reports on the formation of bismuth tungstate by Shang et al. [46], ethanol reacts with Bi^{3+} or MoO_4^{2-} to form a unique $^{C_2H_5\text{-}O}\!\diagdown\!\diagup^{M}$ ($M = Bi^{3+}$ or MoO_4^{2-}) complex through hydrogen bonding between Bi^{3+} (or MoO_4^{2-}) and ethanol. Then the $^{C_2H_5\text{-}O}\!\diagdown\!\diagup^{M}$ ($M = Bi^{3+}$ or MoO_4^{2-}) complex facilitates the formation of Bi_2MoO_6 in the solvothermal procedure possibly following the chemical reactions displayed below:

$$Bi_2O_2(OH)(NO_3) + MoO_4^{2-} + 2CH_3CH_2\text{-}OH \longrightarrow \begin{matrix} C_2H_5\text{-}O \diagdown \\ \qquad\quad M \\ C_2H_5\text{-}O \diagup \end{matrix} \quad (7)$$

$$\begin{matrix} C_2H_5\text{-}O \diagdown \\ \qquad\quad M \\ C_2H_5\text{-}O \diagup \end{matrix} \xrightarrow{solvothermal} Bi_2MoO_6 \quad (8)$$

The effect of TiO_2 can be explained as follows. Based on the XRD results, one comes to the realization that TiO_2 loading is propitious to the formation of Bi_2MoO_6 (Fig. 2). It is likely that butanol and titanium hydroxide is produced during the synthesis process when tetrabutyl titanate is used as TiO_2 precursor. Similar to

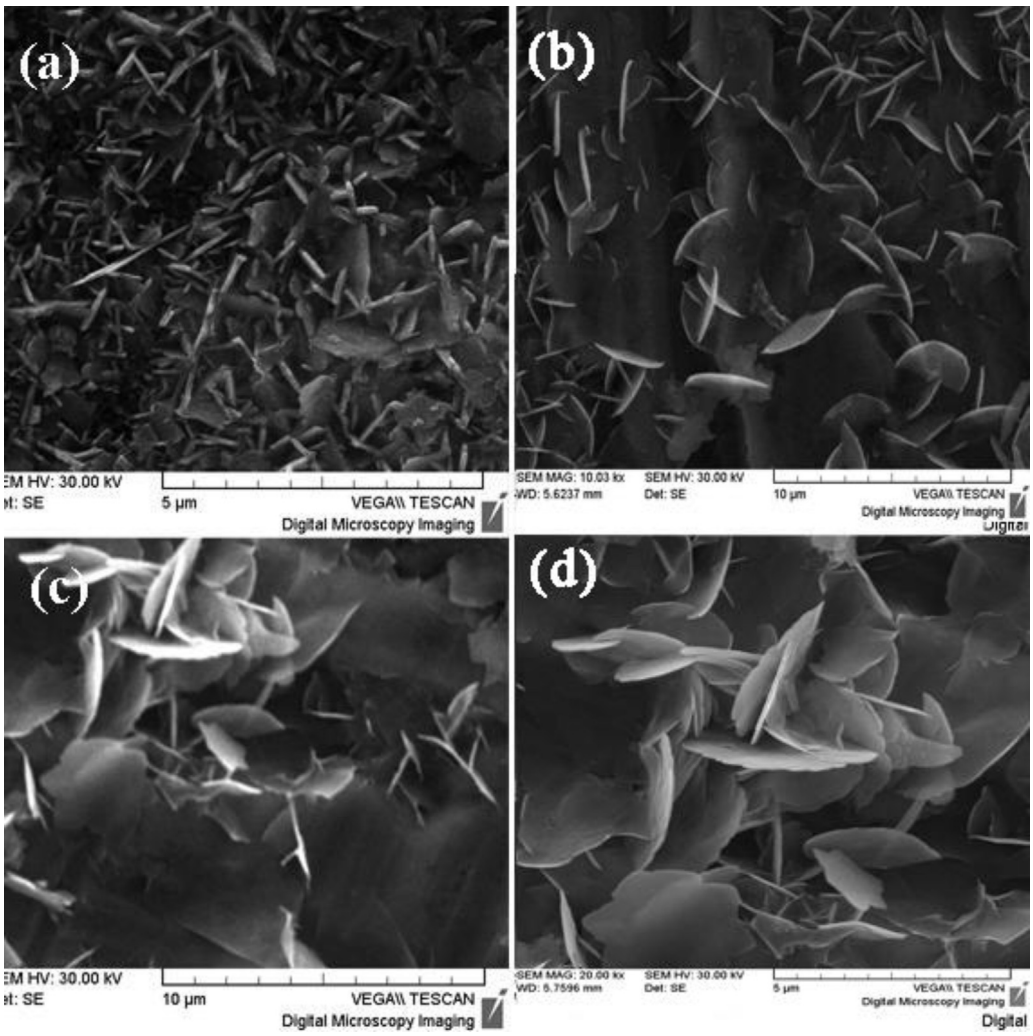

Fig. 6. SEM images of bismuth molybdate loaded (at pH = 7.5) with different TiO_2 contents (a) 2.5%, (b) 5%, (c) 7.5%, and (d) 10%.

ethanol, butanol coordinates with Bi^{3+} or MoO_4^{2-} to form a $^{C_4H_9O}\!\!\diagdown\!\!\diagup^{M}_{C_4H_9O}$ ($M = Bi^{3+}$ or MoO_4^{2-}) complex via hydrogen bonding between Bi^{3+} or MoO_4^{2-} and the hydroxyl group. Hence the increase of TiO_2 loading would mean rise of tetrabutyl titanate content and consequently the rise of butanol content in the solution; the result is increase of Bi_2MoO_6 formation in the solvothermal process:

$$(CH_3CH_2CH_2CH_2O)_4Ti + 2H_2O \longrightarrow Ti(OH)_4 + 4CH_3CH_2CH_2CH_2OH \quad (9)$$

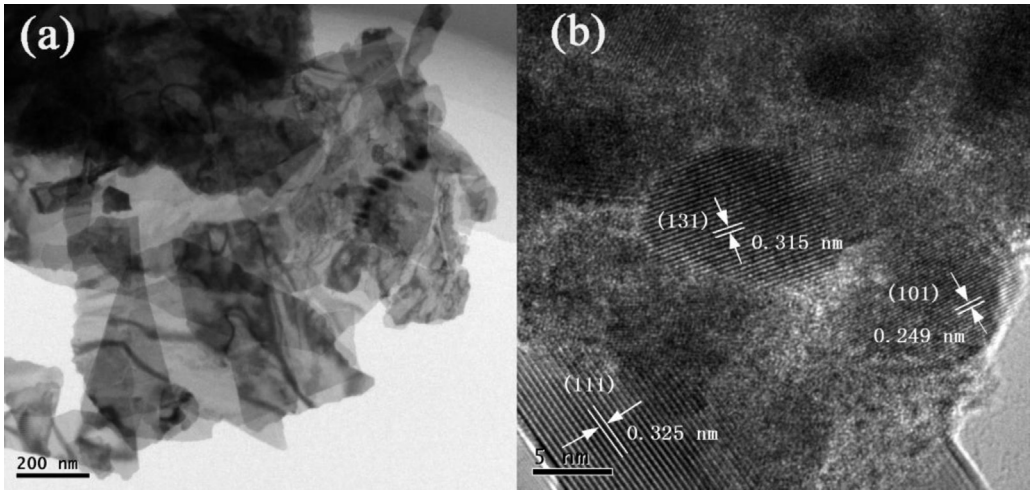

Fig. 7. TEM (a) and HRTEM (b) images of 5TBM.

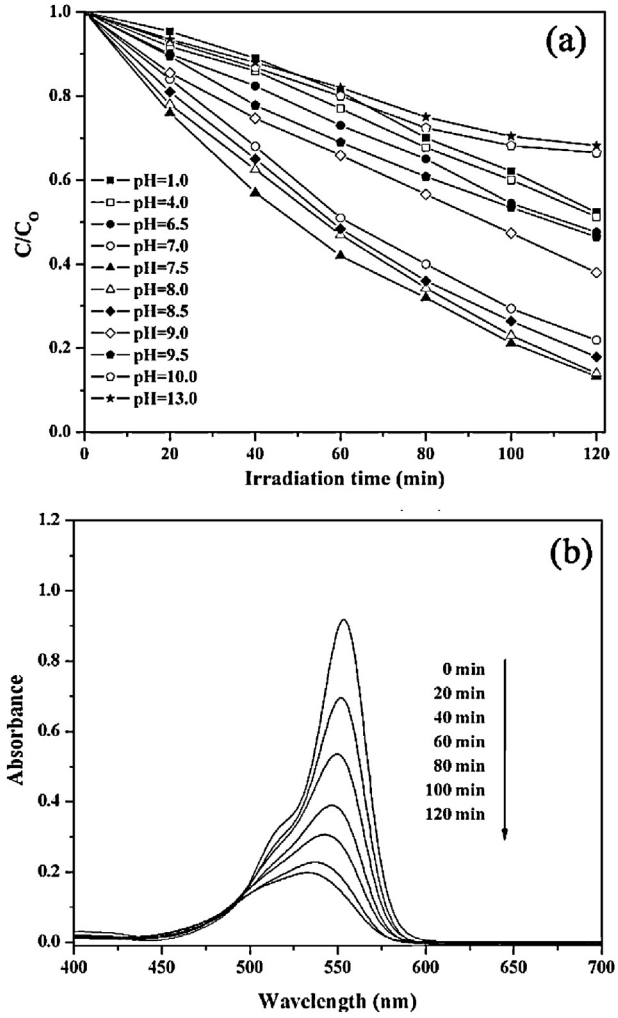

Fig. 8. (a) Photocatalytic degradation of RhB under visible-light irradiation using bismuth molybdate synthesized at different pH values. (b) Absorption spectra of RhB in the presence of $Bi_2MoO_6/Bi_{3.64}Mo_{0.36}O_{6.55}$ (pH = 7.5) as a function of irradiation time.

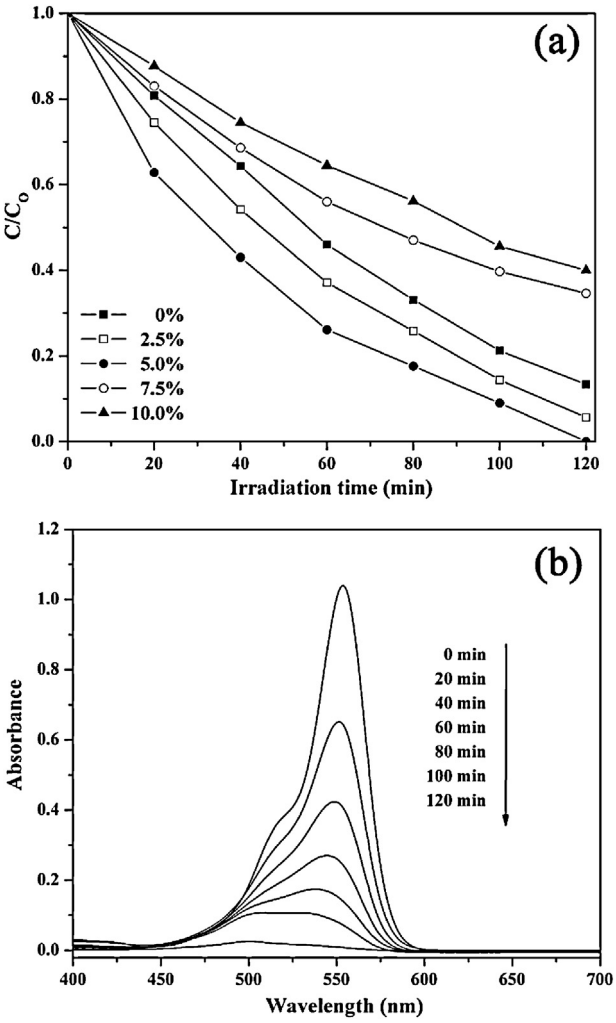

Fig. 9. (a) Photocatalytic degradation of RhB under visible-light irradiation using $Bi_2MoO_6/Bi_{3.64}Mo_{0.36}O_{6.55}$ (pH = 7.5) loaded with different TiO_2 contents. (b) Absorption spectra of RhB in the presence of $5\%TiO_2–Bi_2MoO_6/Bi_{3.64}Mo_{0.36}O_{6.55}$ (pH = 7.5) as a function of irradiation time.

$$Bi_2O_2(OH)(NO_3) + MoO_4^{2-} + 2CH_3CH_2CH_2CH_2\text{-}OH \longrightarrow \begin{matrix} C_4H_9\text{-}O \\ \diagdown \\ M \\ \diagup \\ C_4H_9\text{-}O \end{matrix} \quad (10)$$

$$\begin{matrix} C_4H_9\text{-}O \\ \diagdown \\ M \\ \diagup \\ C_4H_9\text{-}O \end{matrix} \xrightarrow{solvothermal} Bi_2MoO_6 \quad (11)$$

3.3. Photocatalytic results

The photocatalytic activities of the as-prepared materials as reflected in the photodecomposition of Rhodamine B (RhB) and o-nitrophenol under visible light irradiation ($\lambda > 420$ nm) can provide mechanistic information.

The establishment of adsorption/desorption equilibrium was obtained under continuous stirring for 1 h in the dark before the start of degradation reaction. The decrease of light absorption at a wavelength of 554 nm over an aqueous solution of RhB under visible light irradiation would imply decrease of RhB content. Fig. 8a shows plots of RhB photodegradation as a function of irradiation time using different bismuth molybdate samples synthesized under different pH conditions. (C is RhB absorption at a wavelength of 554 nm, and C_0 is RhB absorption after adsorption equilibrium on catalysts.) Fig. 8b displays temporal changes of RhB concentration over the heterostructured $Bi_2MoO_6/Bi_{3.64}Mo_{0.36}O_{6.55}$ composite. It is obvious that the sample prepared at pH = 7.5 is the best in photocatalytic activity: up to 85% of RhB is degraded after 2 h. Based on the results of XRD analysis (Fig. 1), it is known that Bi_2MoO_6 and $Bi_{3.64}Mo_{0.36}O_{6.55}$ co-exist at pH = 7.5 and there is the formation of heterostructure; the outcome is charge-separation efficiency and photocatalytic activity better than those of individual Bi_2MoO_6 and $Bi_{3.64}Mo_{0.36}O_{6.55}$.

In the cases when $Bi_2MoO_6/Bi_{3.64}Mo_{0.36}O_{6.55}$ loaded with different contents of TiO_2 are used for RhB decomposition, there is marked increase of photocatalytic activity with rise of TiO_2 loading (Fig. 9). Best photocatalytic activity is observed over 5TBM. With TiO_2 loading exceeding 5%, the photocatalytic activity declines. Complete degradation of RhB is achieved after 2 h in the presence of 5TBM, while RhB degradation is about 93%, 57% and 50% in the presence of 2.5TBM, 7.5TBM and 10TBM, respectively. In addition, compared to Bi_2MoO_6 and $Bi_{3.64}Mo_{0.36}O_{6.55}$, the bismuth molybdate loaded with TiO_2 ($TiO_2–Bi_2MoO_6$ and $TiO_2–Bi_{3.64}Mo_{0.36}O_{6.55}$) show better photocatalytic activities when TiO_2 loading is less than 5%, and show worse photocatalytic activities when TiO_2 loading

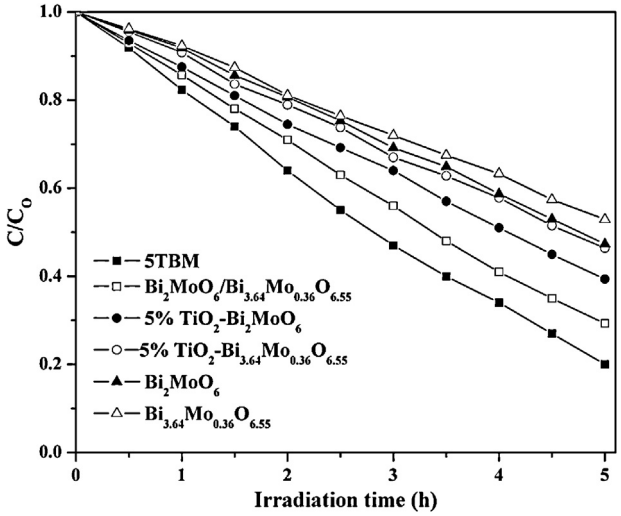

Fig. 10. Photodegradation of o-nitrophenol using different catalysts under visible-light irradiation.

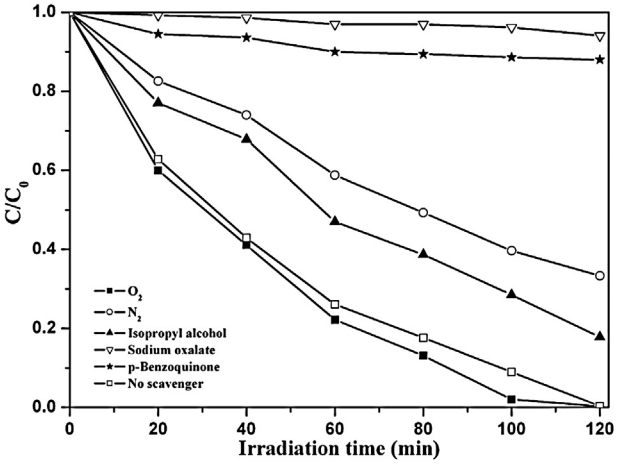

Fig. 11. Photocatalytic degradation of RhB with O_2 and N_2 bubbling or in the presence of different scavengers: isopropyl alcohol (1 mmol/L), sodium oxalate (1 mmol/L) and p-benzoquinone (1 mmol/L) over 5TBM under solar light irradiation.

exceeds 5% (Figs. S7 and S8). In other words, the optimal TiO_2 loading on Bi_2MoO_6 and $Bi_{3.64}Mo_{0.36}O_{6.55}$ is 5% (Figs. S7 and S8). The phenomena that there is change of photocatalytic activity with TiO_2 loading can be explained according to the XRD (Fig. 2) and SEM (Fig. 6) results. Across the TiO_2–Bi_2MoO_6/$Bi_{3.64}Mo_{0.36}O_{6.55}$ samples, the $Bi_{3.64}Mo_{0.36}O_{6.55}$ phase gradually disappears with increase of TiO_2 loading, and completely disappears at a TiO_2 loading of 10%, implying the complete conversion of ternary heterostructured TiO_2–Bi_2MoO_6/$Bi_{3.64}Mo_{0.36}O_{6.55}$ to binary heterostructured TiO_2–Bi_2MoO_6. Also, the crystallinity of TiO_2–Bi_2MoO_6/$Bi_{3.64}Mo_{0.36}O_{6.55}$ is the best at a TiO_2 loading of 5%. As far as the existence and crystallinity of TiO_2–Bi_2MoO_6/$Bi_{3.64}Mo_{0.36}O_{6.55}$ is concerned, 5TBM is the best, and such characteristics of 5TBM can be related to its photocatalytic performance which is the best among the prepared catalysts. We mechanically mixed Bi_2MoO_6/$Bi_{3.64}Mo_{0.36}O_{6.55}$ (95%, based on Ti/Bi molar ratio) with TiO_2 (5%) synthesized by us as well as with commercial P25 (5%). The photodegradation of RhB catalyzed by the mixtures is obviously worse than that by 5TBM (Figure S9). Hence the better performance of 5TBM is considered to be due to the heterojunctions of 5TBM.

o-Nitrophenol is an important intermediate for the syntheses of dyes, pharmaceuticals and agrochemicals. The compound is toxic and not easily biodegradable, and the extensive use of it has caused much environmental concern. It is hence of significance to study the photocatalytic degradation of o-nitrophenol. To further evaluate the photocatalytic activity of the as-prepared materials, the photocatalytic degradation of o-nitrophenol was investigated under the conditions similar to those of RhB degradation (Figs. S10 and 10).

Figs. S10a–S10f reveal the gradual decrease of o-nitrophenol concentration (monitored at 278 nm) over Bi_2MoO_6, $Bi_{3.64}Mo_{0.36}O_{6.55}$, 5%$TiO_2$–$Bi_2MoO_6$, 5TBM, 5%$TiO_2$–$Bi_{3.64}Mo_{0.36}O_{6.55}$, and Bi_2MoO_6/$Bi_{3.64}Mo_{0.36}O_{6.55}$ under irradiation of visible light. Fig. 10 shows that among the four catalysts loaded with TiO_2, 5TBM shows highest degradation rate: up to 83% of o-nitrophenol is degraded after 5 h. In the cases of Bi_2MoO_6/$Bi_{3.64}Mo_{0.36}O_{6.55}$, 5%$TiO_2$–$Bi_2MoO_6$, 5%$TiO_2$–$Bi_{3.64}Mo_{0.36}O_{6.55}$, Bi_2MoO_6, and $Bi_{3.64}Mo_{0.36}O_{6.55}$, o-nitrophenol degradation is ca. 70%, 60% and 50%, 47%, and 40%, respectively. To the best of our knowledge, the photocatalytic activity of 5TBM is the best among the photocatalysts ever reported for o-nitrophenol photodegradtion under visible-light irradiation [47].

Table S2 shows the Brunauer–Emmett–Teller (BET) surface areas of the prepared materials. It is obvious that compared to the samples of bismuth molybdate without TiO_2 loading, those loaded with 5% TiO_2 synthesized under equal pH condition are higher in BET surface area. The BET surface area of 5TBM is about 17.9 m^2/g, whereas those of Bi_2MoO_6, $Bi_{3.64}Mo_{0.36}O_{6.55}$, Bi_2MoO_6/$Bi_{3.64}Mo_{0.36}O_{6.55}$, 5%$TiO_2$–$Bi_2MoO_6$, and 5%$TiO_2$–$Bi_{3.64}Mo_{0.36}O_{6.55}$ are about 4.35, 7.39, 9.59, 10.8, and 13.7 m^2/g, respectively. Thus besides being better in charge separation efficiency, the higher photocatalytic activity of 5TBM can be attributed to its large BET surface area.

3.4. Photodegradation mechanism

It is well known that photoinduced holes, super oxygen free radicals ($^{\bullet}O^{2-}$), and hydroxyl radicals ($^{\bullet}OH$) are extremely active, and it is these species that trigger the oxidation of organic pollutants. To investigate the photocatalytic mechanism, it is important to identify which of these are responsible for photodegradation. We performed trapping experiment using isopropyl alcohol ($^{\bullet}OH$ radical scavenger), p-benzoquinone ($^{\bullet}O^{2-}$ scavenger) and sodium oxalate (hole scavenger) to determine the major reactive species accountable for RhB degradation over the 5TBM catalyst. As shown in Fig. 11, with the addition of sodium oxalate, isopropyl alcohol, and p-benzoquinone, the degradation of RhB is around 5%, 80% and 12%, respectively, in 120 min. Compared to the case of no addition of scavengers (100% degradation in 120 min), one can see that the deceleration of photodegradation activity is in the order: sodium oxalate > p-benzoquinone $\gg$ isopropyl alcohol. The results show that photogenerated holes and $^{\bullet}O^{2-}$ are major species involved in RhB photodegradation. It was also observed that the degradation of RhB is obviously inhibited when N_2 is bubbled into the reaction system but slightly enhanced when N_2 is replaced with O_2. The phenomena reveal that molecular oxygen traps the photoinduced electrons as well as involves in the generation of $^{\bullet}O^{2-}$, and the outcome is enhancement of RhB degradation over 5TBM.

3.5. Mechanism of photocatalytic activity enhancement

Photocurrent measurements were carried out over 5TBM and Bi_2MoO_6/$Bi_{3.64}Mo_{0.36}O_{6.55}$ after deposition on FTO electrodes (Fig. S11). A fast and uniform photocurrent response is observed for each switch-on and switch-off event. The photocurrent transients at the two electrodes are different in shape, and the

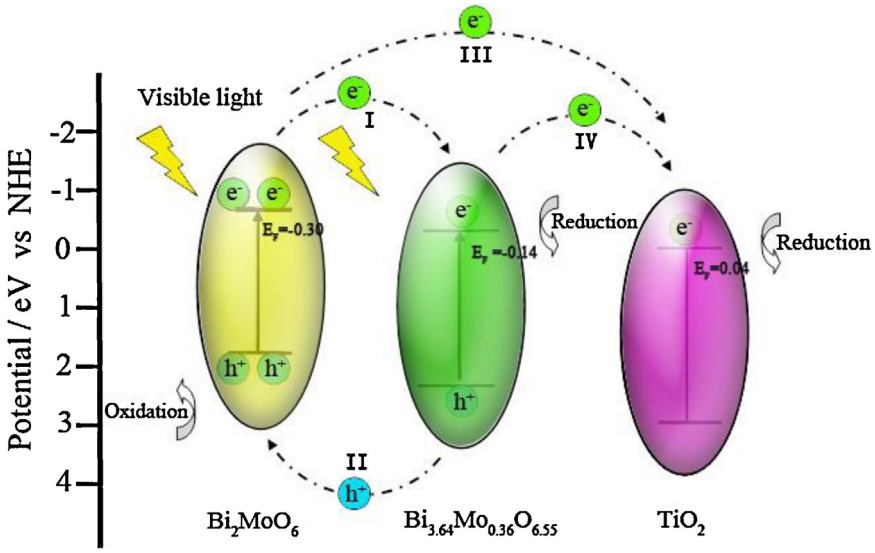

Fig. 12. Energy band diagram and photocatalytic scheme of the TiO_2–Bi_2MoO_6/$Bi_{3.64}Mo_{0.36}O_{6.55}$ heterostructured system.

photo-responses are reversible. It is observed that the photocurrent of the 5TBM electrode is about nine times that of the Bi_2MoO_6/$Bi_{3.64}Mo_{0.36}O_{6.55}$ electrode. The result indicates that the separation efficiency of photoinduced electrons and holes is improved through electronic interaction among TiO_2, Bi_2MoO_6 and $Bi_{3.64}Mo_{0.36}O_{6.55}$. The photocurrent responses of Bi_2MoO_6, $Bi_{3.64}Mo_{0.36}O_{6.55}$, 5%$TiO_2$–$Bi_2MoO_6$ and 5%TiO_2–$Bi_{3.64}Mo_{0.36}O_{6.55}$ are weak, in consistent with their photocatalytic activities. The high photocurrent response of 5TBM can be related to the good photocatalytic activity of 5TBM as compared to those of the bismuth molybdates with or without TiO_2 loading.

Furthermore, the electrochemical properties of the photocatalysts were studied using a standard three-electrode cell. Fig. S12 shows the Mott–Sckottky (MS) plots with Bi_2MoO_6, $Bi_{3.64}Mo_{0.36}O_{6.55}$ and TiO_2 being working electrode (0.5 M K_2SO_4 as electrolyte). Reversed sigmoidal plots are observed with an overall shape typical of n-type semiconductors. The V_{fb} as calculated from the x intercepts of the linear region are found to be −0.54, −0.38 and −0.10 eV vs. SCE (equivalent to −0.30, −0.14 and 0.14 eV vs. NHE, respectively) for Bi_2MoO_6, $Bi_{3.64}Mo_{0.36}O_{6.55}$ and TiO_2, respectively, in consistent with the V_{fb} value (−0.32 V vs. NHE) of Bi_2MoO_6 calculated by Long et al. [48]. It is known that the flat band potential of n-type semiconductor equals to the Fermi Level (E_F). Therefore, the E_F values of Bi_2MoO_6, $Bi_{3.64}Mo_{0.36}O_{6.55}$ and TiO_2 are −0.30, −0.14 and 0.14 eV, respectively. Accordingly, the CB of Bi_2MoO_6, $Bi_{3.64}Mo_{0.36}O_{6.55}$ and TiO_2 can be calculated as −0.50, −0.34 and −0.06 eV, respectively [49,50]. The band positions can be calculated by the following empirical formulas: $E_{CB} = E_{VB} - E_g$, and the valence band (VB) of Bi_2MoO_6, $Bi_{3.64}Mo_{0.36}O_{6.55}$ and TiO_2 are 2.05, 2.34 and 3.14 eV, respectively. Based on the above results, the energy band diagram of heterostructured TiO_2–Bi_2MoO_6/$Bi_{3.64}Mo_{0.36}O_{6.55}$ is presented in Fig. 12. When the heterostructured TiO_2–Bi_2MoO_6/$Bi_{3.64}Mo_{0.36}O_{6.55}$ are irradiated by visible light with energy equal or higher than the band gap of either Bi_2MoO_6 or $Bi_{3.64}Mo_{0.36}O_{6.55}$, there will be the generation of holes in its VB and electrons in its CB, respectively.

For the heterostructured photocatalysts, four possible pathways might be considered for the generation of photogenerated charge carriers. First, when Bi_2MoO_6 and $Bi_{3.64}Mo_{0.36}O_{6.55}$ are simultaneously excited under visible light irradiation, the photogenerated electrons in the CB of Bi_2MoO_6 flow into the CB of $Bi_{3.64}Mo_{0.36}O_{6.55}$ (electron transfer I: $Bi_2MoO_6 \rightarrow Bi_{3.64}Mo_{0.36}O_{6.55}$) through the Schottky barrier since the CB of Bi_2MoO_6 is more negative than that of $Bi_{3.64}Mo_{0.36}O_{6.55}$ [19,51,52]. Simultaneously, the photogenerated holes in the VB of $Bi_{3.64}Mo_{0.36}O_{6.55}$ flow into the VB of Bi_2MoO_6 (electron transfer II: $Bi_{3.64}Mo_{0.36}O_{6.55} \rightarrow Bi_2MoO_6$) through the Schottky barrier because the VB of Bi_2MoO_6 is more negative than that of $Bi_{3.64}Mo_{0.36}O_{6.55}$. It is envisaged that the processes of electron transfer I and II are faster than the electron–hole recombination process between the VB and CB of Bi_2MoO_6 or $Bi_{3.64}Mo_{0.36}O_{6.55}$. Thus, the CB-electrons of Bi_2MoO_6 can be stored in $Bi_{3.64}Mo_{0.36}O_{6.55}$ while the VB holes of $Bi_{3.64}Mo_{0.36}O_{6.55}$ can be stored in Bi_2MoO_6, inhibiting the recombination of electrons and holes as a result. This is the reason why the heterostructured Bi_2MoO_6/$Bi_{3.64}Mo_{0.36}O_{6.55}$ performs better than the individual Bi_2MoO_6 and $Bi_{3.64}Mo_{0.36}O_{6.55}$ in photocatalytic degradation of RhB and o-nitrophenol as demonstrated in Figs. 8 and 10, respectively.

Second, in the heterostructured TiO_2–Bi_2MoO_6 system, Bi_2MoO_6 is activated but TiO_2 is not activated under visible light irradiation. There is the transfer of photogenerated electrons in the CB of Bi_2MoO_6 into the CB of TiO_2 (electron transfer III: $Bi_2MoO_6 \rightarrow TiO_2$) through the Schottky barrier because the CB of Bi_2MoO_6 is more negative than that of TiO_2, inhibiting the electron–hole recombination between the VB and CB of Bi_2MoO_6 as a result. Analogous to the heterostructured TiO_2–Bi_2MoO_6 system, the heterostructured TiO_2–$Bi_{3.64}Mo_{0.36}O_{6.55}$ system has similar pathways of electrons transfer (Fig. 12, electrons transfer IV: $Bi_{3.64}Mo_{0.36}O_{6.55} \rightarrow TiO_2$). This is the reason why heterostructured 5%TiO_2–Bi_2MoO_6 and 5%TiO_2–$Bi_{3.64}Mo_{0.36}O_{6.55}$ exhibit better photocatalytic activities than the individual Bi_2MoO_6 and $Bi_{3.64}Mo_{0.36}O_{6.55}$ for the degradation of RhB and o-nitrophenol as demonstrated in Figs. S7, S8 and 10.

It is envisaged that the above four pathways (electrons transfer I–VI) are involved in the photodegradation of RhB and o-nitrophenol using ternary heterostructured TiO_2–Bi_2MoO_6/$Bi_{3.64}Mo_{0.36}O_{6.55}$. This new understanding of photocatalytic mechanism explains why the ternary heterostructured 5%TiO_2–Bi_2MoO_6/$Bi_{3.64}Mo_{0.36}O_{6.55}$ performs the best among the investigated photocatalysts (i.e. Bi_2MoO_6, $Bi_{3.64}Mo_{0.36}O_{6.55}$, TiO_2–Bi_2MoO_6, TiO_2–$Bi_{3.64}Mo_{0.36}O_{6.55}$, and TiO_2–Bi_2MoO_6/$Bi_{3.64}Mo_{0.36}O_{6.55}$) as demonstrated in Figs. 8–10.

4. Conclusions

Ternary heterostructured photocatalysts TiO_2–Bi_2MoO_6/$Bi_{3.64}Mo_{0.36}O_{6.55}$, as well as Bi_2MoO_6, $Bi_{3.64}Mo_{0.36}O_{6.55}$ and Bi_2MoO_6/$Bi_{3.64}Mo_{0.36}O_{6.55}$, TiO_2–Bi_2MoO_6 and TiO_2–$Bi_{3.64}Mo_{0.36}O_{6.55}$ composites were prepared using a solvothermal method. The binary or ternary heterostructured composites were synthesized with controllable composition, structure and morphology without the use of template. The experimental results reveal that the composition, structure (or phase) and morphology of bismuth molybdate can be controlled by regulating the pH value, solvent composition and TiO_2 loading adopted in catalyst preparation. Based on the phenomena observed related to the evolution of composition, morphology and structure, we propose a reasonable mechanism for the formation of the photocatalysts. In photocatalytic degradation of RhB and o-nitrophenol over the as-prepared catalysts, it is observed that photocatalytic activities are closely related to the composition, morphology and structure of catalysts synthesized under different conditions. Integrating the synergetic effect of TiO_2/Bi_2MoO_6, TiO_2/$Bi_{3.64}Mo_{0.36}O_{6.55}$ and Bi_2MoO_6/$Bi_{3.64}Mo_{0.36}O_{6.55}$, the heterostructued TiO_2–Bi_2MoO_6/$Bi_{3.64}Mo_{0.36}O_{6.55}$ catalyst is superior in transferring the photogenerated electrons and holes, thereby improving photocatalytic efficiency. We propose a mechanism for the photocatalytic activity observed over the heterostructured materials. It is a new mode of photocatalytic reaction giving explanation for the effectiveness of interfacial charge transfer as well as for the photocatalytic efficiency of the ternary heterostructured composites.

Acknowledgements

We gratefully acknowledge the financial support of the NSF of China (20801026, 51238002 and 51272099), the NSF of Jiangxi Province (20114BAB203005), and the Aviation Science Foundation of China (2008ZF56012), and Foundation of State Key Laboratory of Structural Chemistry (20100015).

Appendix A. Supplementary data

Supplementary data associated with this article can be found, in the online version, at http://dx.doi.org/10.1016/j.apcatb.2013.04.057.

References

[1] H.Q. Li, J. Qu, Q.Z. Cui, H.B. Xu, H.M. Luo, M.F. Chi, R.A. Meisner, W. Wang, S. Dai, Journal of Materials Chemistry 21 (2011) 9487.
[2] X.C. Wang, K. Maeda, A. Thomas, K. Takanabe, G. Xin, J.M. Carlsson, K. Domen, M. Antonietti, Nature Materials 8 (2009) 76.
[3] F.T. Wagner, G.A. Somorjai, Nature 285 (1980) 559.
[4] Z.X. Jiang, H.Y. Lu, Y.N. Zhang, C. Li, Chinese Journal of Catalysis 32 (2011) 707.
[5] X.J. Liu, L.K. Pan, T. Lv, T. Lu, G. Zhu, Z. Sun, C.Q. Sun, Catalysis Science and Technology 1 (2011) 1189.
[6] J. Zhang, S.L. Liu, J.G. Yu, M. Jaroniec, Journal of Materials Chemistry 21 (2011) 14655.
[7] A. Fujishima, K. Honda, Nature 238 (1972) 37.
[8] M.Y. Zhu, G.W. Diao, Journal of Physical Chemistry C 115 (2011) 18923.
[9] S.D. Sun, F.Y. Zhou, L.Q. Wang, X.P. Song, Z.M. Yang, Crystal Growth and Design 10 (2010) 541.
[10] X.Y. Sun, J. Lin, Journal of Physical Chemistry C 113 (2009) 4970.
[11] J.J. Wu, F.Q. Huang, X.J. Lv, P. Chen, CrystEngComm 13 (2011) 3920.
[12] T. Saison, N. Chemin, C. Chanéac, O. Durupthy, V. Ruaux, L. Mariey, F. Maugé, P. Beaunier, J.P. Jolivet, Journal of Physical Chemistry C 115 (2011) 5657.
[13] L.P. Zhu, G.H. Liao, N.C. Bing, L.L. Wang, Y. Yang, H.Y. Xie, CrystEngComm 12 (2010) 3791.
[14] N. Serpone, E. Borgarello, M. Grätzel, Journal of the Chemical Society-Chemical Communications 1 (1984) 342.
[15] D.N. Ke, H.J. Liu, T.Y. Peng, X. Liu, K. Dai, Materials Letters 62 (2008) 447.
[16] X. Zhang, L.Z. Zhang, T.F. Xie, D.J. Wang, Journal of Physical Chemistry C 113 (2009) 7371.
[17] T.B. Li, G. Chen, C. Zhou, Z.Y. Shen, R.C. Jin, J.X. Sun, Dalton Transactions 40 (2011) 6751.
[18] M.S. Gui, W.D. Zhang, Q.X. Su, C.H. Chen, Journal of Solid State Chemistry 184 (2011) 1977.
[19] Y.Y. Li, J.S. Wang, H.C. Yao, L.Y. Dang, Z.J. Li, Catalysis Communications 12 (2011) 660.
[20] J. Ren, W.Z. Wang, M. Shang, S.M. Sun, E.P. Gao, ACS Applied Materials and Interfaces 3 (2011) 2529.
[21] H. Tada, T. Mitsui, T. Kiyonaga, T. Akita, K. Tanaka, Nature Materials 5 (2006) 782.
[22] C. Hu, Y.Q. Lan, J.H. Qu, X.X. Hu, A.M. Wang, Journal of Physical Chemistry B 110 (2006) 4066.
[23] H.F. Cheng, B.B. Huang, P. Wang, Z.Y. Wang, Z.Z. Lou, J.P. Wang, X.Y. Qin, X.Y. Zhang, Y. Dai, Chemical Communications 47 (2011) 7054.
[24] Y.G. Xu, H. Xu, H.M. Li, J.X. Xia, C.T. Liu, L. Liu, Journal of Alloys and Compounds 509 (2011) 3286.
[25] L.S. Zhang, K.H. Wong, Z.G. Chen, J.C. Yu, J.C. Zhao, C. Hu, C.Y. Chan, P.K. Wong, Applied Catalysis A 363 (2009) 221.
[26] Y. Wang, L. Cai, Y. Li, Y. Tang, C. Xie, Physica E 43 (2010) 503.
[27] A.K. Chakraborty, S.B. Rawal, S.Y. Han, S.Y. Chai, W.I. Lee, Applied Catalysis A-General 407 (2011) 217.
[28] J. Cao, B. Xu, B. Luo, H. Lin, S. Chen, Applied Surface Science 257 (2011) 7083.
[29] Z. Shen, G. Chen, Q. Wang, Y. Yu, C. Zhou, Y. Wang, Nanoscale 4 (2012) 2010.
[30] C.M.C. Vera, R. Aragona, Journal of Solid State Chemistry 181 (2008) 1075.
[31] L. Zhou, W.Z. Wang, L.S. Zhang, Journal of Molecular Catalysis A: Chemical 268 (2007) 195.
[32] M.S. Islam, S. Lazure, R.N. Vannier, G. Nowogrocki, G.J. Mairesse, Journal of Materials Chemistry 8 (1998) 655.
[33] H.H. Li, C.Y. Liu, K.W. Li, H. Wang, Journal of Materials Science 43 (2008) 7026.
[34] X. Zhao, T. Xu, W. Yao, Y. Zhu, Applied Surface Science 255 (2009) 8036.
[35] G.H. Tian, Y.J. Chen, W. Zhou, K. Pan, Y.Z. Dong, H.G. Fu, Journal of Materials Chemistry 21 (2011) 887.
[36] X. Zhao, J. Qu, H. Liu, Z. Qiang, R. Liu, C. Hu, Applied Catalysis B: Environmental 91 (2009) 539.
[37] R. Murugan, Physica B 352 (2004) 227.
[38] T.P. Cao, Y.J. Li, C.H. Wang, C.L. Shao, Y.C. Liu, Langmuir 27 (2011) 2946.
[39] X.L. Wang, S.O. Pehkonen, J.K. Ramo, M.J. Vaananen, J.G. Highfielde, K. Laasonenf, Catalysis Science and Technology 2 (2012) 784.
[40] F. Amano, K. Nogami, R. Abe, B.J. Ohtani, Physical Chemistry C 112 (2008) 9320–9326.
[41] Y. Wang, Y. Wang, Y. Meng, H. Ding, Y. Shan, X. Zhao, X.J. Tang, Physical Chemistry C 112 (2008) 6620–6626.
[42] M.J. Zhang, C.L. Shao, J.B. Mu, Z.Y. Zhang, Z.C. Guo, P. Zhang, Y.C. Liu, CrystEngComm 14 (2012) 605.
[43] W.W. Wendlandt, H.G. Hecht, Reflectance Spectroscopy, Interscience Publishers, New York, 1966.
[44] L.S. Zhang, H.L. Wang, Z.G. Chen, P.K. Wong, J.S. Liu, Applied Catalysis B: Environmental 106 (2011) 1.
[45] Y. Tian, G.M. Hua, W. Xu, N. Li, M. Fang, L.D. Zhang, Journal of Alloys and Compounds 509 (2011) 724.
[46] M. Shang, W.Z. Wang, H.L. Xu, Crystal Growth and Design 9 (2009) 991.
[47] F.R. Zaggout, N.A. Ghalwa, Journal of Environment Management 86 (2008) 291.
[48] M.C. Long, W.M. Cai, H. Kisch, Chemical Physics Letters 461 (2008) 102.
[49] A. Ishikawa, T. Takata, J.N. Kondo, M. Hara, H. Kobayashi, K. Domen, Journal of the American Chemical Society 124 (2002) 13547.
[50] E.P. Gao, W.Z. Wang, M. Shang, J.H. Xu, Physical Chemistry Chemical Physics 13 (2011) 2887.
[51] J. Cao, B.Y. Xu, B.D. Luo, H.L. Lin, S.F. Chen, Catalysis Communications 13 (2011) 63.
[52] F. Zhou, R. Shi, Y. Zhu, Journal of Molecular Catalysis A: Chemical 340 (2011) 77.